

Article

## Influence of Annealing on Mechanical Properties of Al-20Si Processed by Selective Laser Melting

Pan Ma <sup>1,2</sup>, Konda G. Prashanth <sup>2</sup>, Sergio Scudino <sup>2,\*</sup>, Yandong Jia <sup>1,2</sup>, Hongwei Wang <sup>1</sup>, Chunming Zou <sup>1</sup>, Zunjie Wei <sup>1,\*</sup> and Jürgen Eckert <sup>2,3</sup>

<sup>1</sup> School of Materials Science and Engineering, Harbin Institute of Technology, Harbin 150001, China; E-Mails: mapanhit@hotmail.com (P.M.); yandongjia@outlook.com (Y.J.); wanghw@hit.edu.cn (H.W.); zoucm@hit.edu.cn (C.Z.)

<sup>2</sup> IFW Dresden, Institut für Komplexe Materialien, Postfach 27 01 16, D-01171 Dresden, Germany; E-Mails: k.g.prashanth@ifw-dresden.de (K.G.P.); j.eckert@ifw-dresden.de (J.E.)

<sup>3</sup> TU Dresden, Institut für Werkstoffwissenschaft, D-01062 Dresden, Germany

\* Authors to whom correspondence should be addressed; E-Mails: s.scudino@ifw-dresden.de (S.S.); weizj@hit.edu.cn (Z.W.); Tel.: +49-351-4659-838 (S.S.); +86-451-8640-3150 (Z.W.); Fax: +49-351-4659-452 (S.S.); +86-451-8641-8131 (Z.W.).

Received: 17 December 2013; in revised form: 12 January 2014 / Accepted: 22 January 2014 /

Published: 27 January 2014

---

**Abstract:** The microstructure and mechanical properties of Al-20Si produced by selective laser melting (SLM) are investigated for different heat treatment conditions. As a result of the high cooling rate during processing, the as-built SLM material displays a microstructure consisting of a supersaturated Al(Si) solid solution along with heavily refined eutectic Si and Si particles. The Si particles become coarser, and the eutectic Si gradually changes its morphology from fibrous to plate-like shape with increasing annealing temperature. The microstructural variations occurring during heat treatment significantly affect the mechanical behavior of the samples. The yield and ultimate strengths decrease from 374 and 506 MPa for the as-built SLM material to 162 and 252 MPa for the sample annealed at 673 K, whereas the ductility increases from 1.6 to 8.7%. This offers the possibility to tune microstructure and corresponding properties of the Al-20Si SLM parts to meet specific requirements.

**Keywords:** Al-20Si alloy; selective laser melting (SLM); heat treatment; microstructure; mechanical properties

---

## 1. Introduction

Selective laser melting (SLM) is an additive manufacturing technique that produces three dimensional parts directly from CAD data [1–3]. Due to its flexibility in feedstock and shapes, SLM permits the fabrication of complex and intricate geometries with a high degree of accuracy. The combined features of high design flexibility, excellent process capabilities, and high material utilization rates make this technique of considerable interest among both the research and industrial communities [4–7].

Al-based alloys are of significant importance as lightweight structural materials because of the combination of high strength and low density [8–10] and SLM is particularly attractive for the production of Al-based components with customized geometries and properties. In addition, the high cooling rate characterizing SLM processing can produce very fine microstructures [11,12] or even metastable phases, such as bulk metallic glasses [13]. For example, Thijs *et al.* [14] have reported that an extremely fine microstructure and a high hardness can be obtained for AlSi10Mg produced by SLM. Similarly, Prashanth *et al.* [15] have observed an extremely fine cellular structure for Al-12Si alloy processed by SLM. Such a microstructure leads to yield and tensile strengths which are respectively four and two times higher than the corresponding values of the cast material [15]. Moreover, the mechanical behaviour of the Al-12Si SLM material can be tuned within a wide range of strength and ductility through the proper annealing treatments [15].

Hypereutectic Al-Si alloys have wide applications in the automobile and aerospace sectors owing to their high wear and corrosion resistance, low density, high thermal stability, good thermal conductivity and machinability [16–19]. Unfortunately, the SLM research on Al-Si alloys is focused on the hypoeutectic regime and no reports are available on the processing and mechanical properties of the hypereutectic Al-Si SLM alloys. Accordingly, in this work the hypereutectic Al-20Si alloy has been produced by SLM. The microstructure and mechanical behavior of the samples have been investigated in detail and are compared with the samples of the same composition produced by conventional routes. Finally, the effect of heat treatment on the microstructure and resulting mechanical properties has been systematically studied.

## 2. Results and Discussion

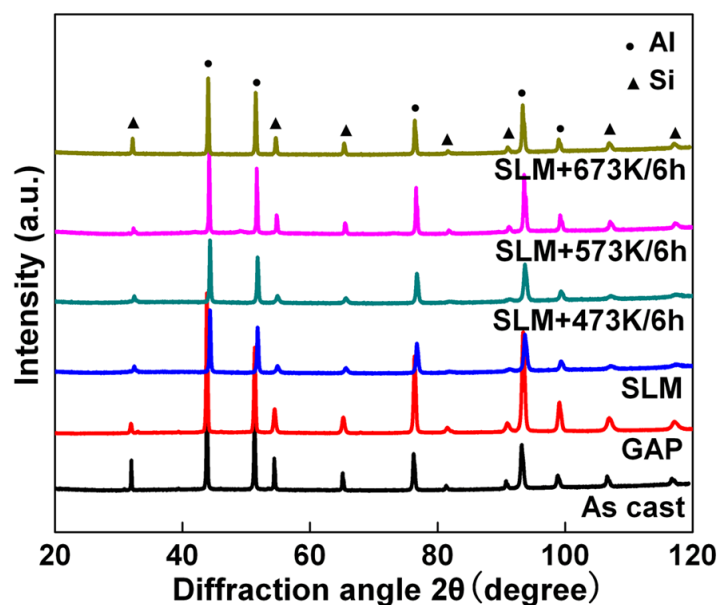
Figure 1 shows the XRD patterns of the Al-20Si gas atomized powders (GAP), as-cast rod, as-built SLM material and heat treated SLM specimens. The diffraction peaks belong to Al and Si only and no other peaks are detected. The Al peaks of the as-SLM sample shift to higher angles compared to both GAP and cast rod. This indicates a significant increase of the Si solid solubility in Al for the SLM material. Indeed, the solubility of Si in Al, evaluated according to the linear relationship between the lattice parameter of Al ( $a$ ) and the atomic fraction of silicon ( $X_{Si}$ ) [20]:

$$a = 0.40491 - 0.0174X_{Si}^2 \quad (1)$$

is found to be 8.75 wt.% for the as-SLM material, which is much higher than the equilibrium solid solubility of Si in Al at room temperature (about 0.05 wt.% [21,22]). Moreover, the intensity of the Si peaks is reduced, as already observed for Al-12Si processed by SLM [15], corroborating that a large amount of Si atoms is dissolved into the Al lattice. The diffraction peaks of Al shift to lower angles

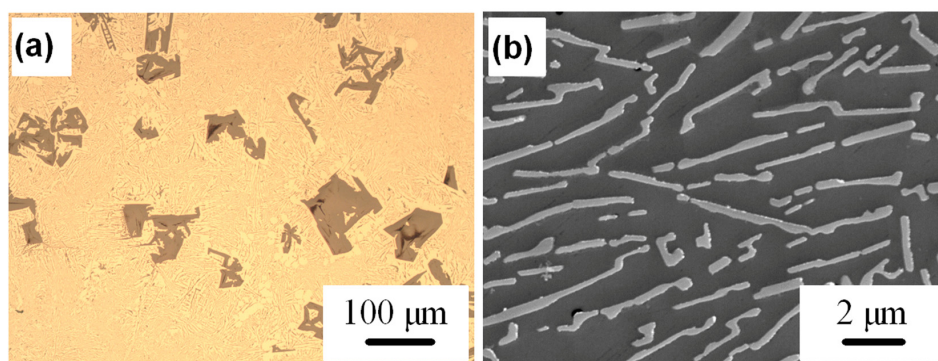
with increasing the annealing temperature that, according to Equation (1), corresponds to a residual Si in Al of 3.11, 0.75 and 0.48 wt.% for the heat treatment carried out at 473, 573, and 673 K, respectively. The intensity of the Si also increases gradually, which further indicates that Si diffuses out of Al as a result of the heat treatment.

**Figure 1.** X-ray diffraction (XRD) patterns of the Al-20Si samples processed at different conditions.



The typical microstructure of cast Al-20Si alloy is shown in Figure 2. The microstructure is composed of primary Si particles (dark particles in Figure 2a) and of eutectic Al-Si (Figure 2b). The primary Si particles, with polygonal morphology and size of about 60–80  $\mu\text{m}$ , have non-uniform distribution in the matrix. Also, it can be observed that the eutectic silicon shows a coarse acicular morphology with size of  $3 \pm 0.2 \mu\text{m}$ .

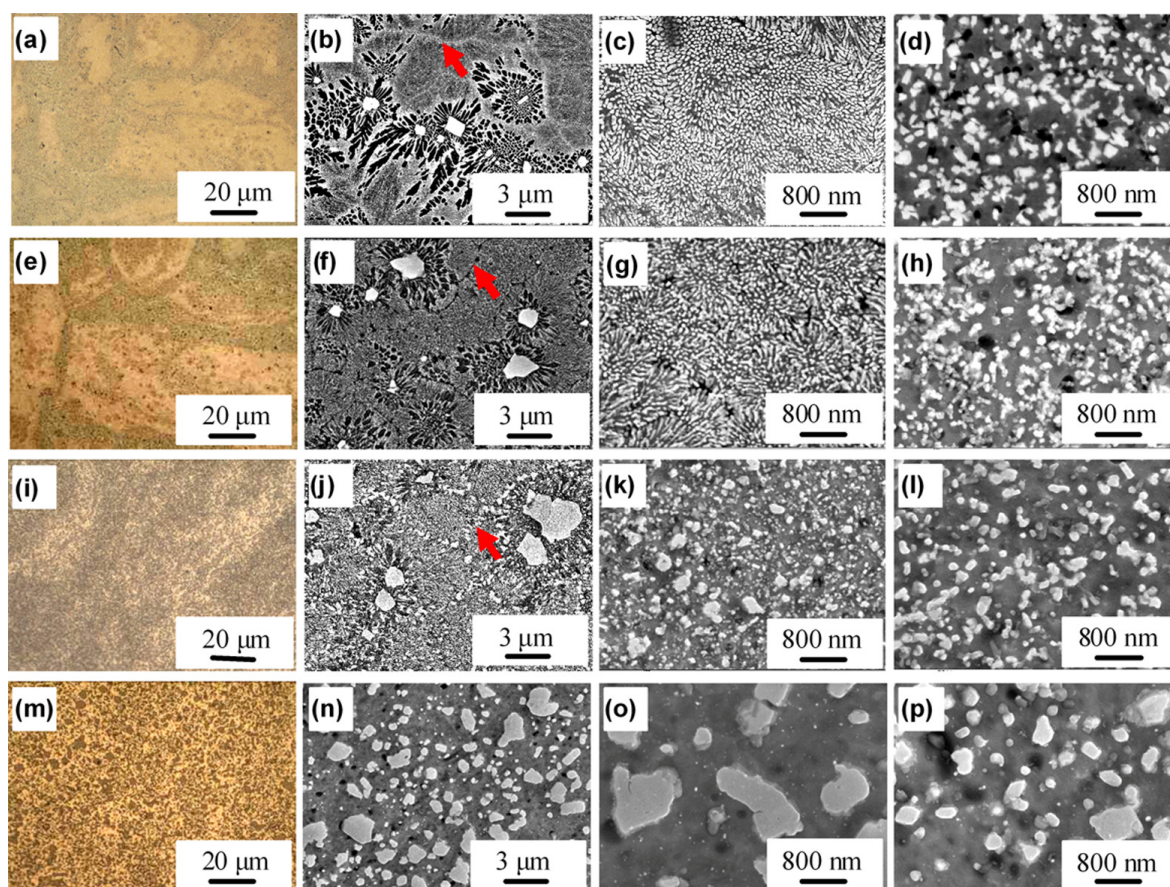
**Figure 2.** (a) Microstructure of as cast Al-20Si alloy, and (b) high magnification micrograph showing the eutectic Al-Si.



The microstructure of the as-built SLM material and heat-treated SLM samples are shown in Figure 3a–p. The microstructure of the as-built SLM sample (Figure 3a) is non-homogenous and displays the typical laser tracks, as already observed for the SLM Al-12Si alloy [15]. The laser tracks

can be divided into two main areas: the track cores and the hatch overlaps, where two different laser tracks are overlapped and where the material is melted two times [15]. The structure within the track cores consists of three zones: (1) polygonal Si particles (white particles in Figure 3b); (2) Al grains (dark grains radiating from the Si particles in Figure 3b) and (3) the fine Al-Si eutectic (Figure 3c). The average size of the Si particles is below 1  $\mu\text{m}$  and is significantly smaller than for the corresponding cast sample (60–80  $\mu\text{m}$ ); moreover, the eutectic structure has fine fibrous shape (in contrast to the long acicular morphology of the cast sample, Figure 2b) and it is partitioned by grain boundaries (indicated by a red arrow in Figure 3b). On the other hand, the hatch overlaps display plate-like Si particles with average size of about 230 nm and no sign of eutectic structure (Figure 3d). During the SLM process, the diffusion of silicon may be hindered due to the rapid solidification. Therefore, the growth of silicon phase is limited, leading to finer Si particles.

**Figure 3.** Microstructure of the Al-20Si selective laser melting (SLM) samples: (a–d) as-built SLM material and SLM samples annealed for 6 h at (e–h) 473, (i–l) 573, (m–p) 673 K.



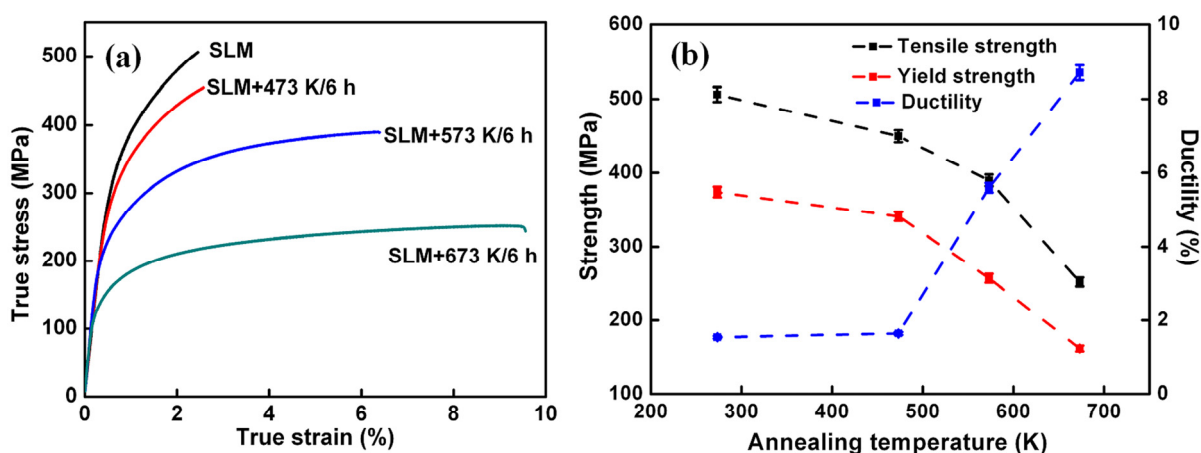
The solidification process in the track cores during SLM of Al-20Si can be described as follows: the Si phase with higher melting point nucleates firstly in the form of particles most likely by a heterogeneous nucleation mechanism. The Si particles then grow and reject the solvent Al into the surrounding undercooled melt, which is thus significantly enriched in Al. The  $\alpha$ -Al phase can then nucleate and grow in the Si depleted zone around the Si particles, consequently arresting the growth of the Si particles. The growth of the  $\alpha$ -Al phase results in an increased Si concentration in the residual

liquid to an extent that, eventually, may shift the composition of the liquid phase into the eutectic zone. This results in the cooperative growth mechanism between Si and Al that yields the eutectic phase in the latter stages of solidification [23–25]. The formation of the fibrous eutectic structure can be attributed to the large energy density imposed by the laser scanning on the surface of the material along with the high heat conductivity of Al. A very steep temperature gradient may be produced on the surface of the melted metal [25], consequently, the laser melting treatment induces a high undercooling which may promote heavy branching of the Si crystal into the fibrous morphology [26].

With increasing the annealing temperature, the hatch overlaps are no longer easily observable and the microstructure becomes coarser but more homogeneous. Both eutectic and particulate Si display little change in shape and size after heat treatment at 473 K (Figure 3g–h). The grain boundaries become more evident compared with the as-built SLM sample (see red arrow in Figure 3f). After heat treatment at 573 K, the fibrous eutectic structure is absent and the microstructure consists of discrete Si particles (Figure 3j,k). This is particularly evident in Figure 3j, where Si particles precipitate along the grain boundaries. The Si particles resulting from the transformation of the eutectic microstructure show considerable coarsening after heat treatment at 673 K (Figure 3n,o).

The Si particles along the hatch overlaps become coarser with increasing the annealing temperature. The size of the Si particles in the as-built SLM sample is extremely fine (230 nm). The resulting large total interfacial energy, which provides a high driving force for coarsening, results in significant growth of the Si particles. This is in accordance with the results observed for Al-12Si SLM samples after annealing [15]. During the annealing process, a significant amount of Si is rejected from the Al phase, as indicated by the shift of the Al diffraction peaks in Figure 1. The availability of extra Si resulting from the supersaturation of Si may thus provide an additional contribution to the driving force for the growth of the Si particles.

**Figure 4.** (a) Tensile stress-strain curves for the different Al-20Si alloys processed by SLM, and (b) corresponding mechanical data (error bars represent the standard deviation).



The room temperature tensile stress-strain curves for the different Al-20Si SLM samples are shown in Figure 4a and the corresponding results are given in Figure 4b. The as-built SLM specimen exhibits the highest yield and ultimate strengths ( $374 \pm 4$  MPa and  $506 \pm 5$  MPa, respectively) along with ductility of  $1.6\% \pm 0.2\%$ . The tensile properties of the same alloy processed by other methods are

given in Table 1. It can be observed that the Al-20Si alloy processed by SLM shows the highest strength among the alloys but a relatively limited ductility.

**Table 1.** Tensile properties of Al-20Si alloys processed by different methods. (YS = yield strength; UTS = ultimate tensile strength).

Preparation methods	YS (MPa)	UTS (MPa)	Ductility (%)
As cast [27]	105	162	4.6
As cast [28]	95	120	0.37
As cast [29]	-	91.5	0.49
Ultrasonic treated [28]	80	130	1.2
Extruded [30]	155	190	3.6
Extruded [31]	-	280	>30
Extruded + ECAP [31]	-	350	>30
RS + Wrought [27]	131	210	19.7
As cast + wrought [27]	118	177	7.7

The heat treatment has a definite influence on the mechanical properties of the Al-20Si SLM material. For the sample heat treated at 473 K, there is a marginal decrease in both yield and ultimate strengths; however, no distinct change in ductility is observed. With further increase of the annealing temperature, the strength is reduced and the ductility increases significantly. For example, when the annealing temperature is increased to 673 K, the sample displays the lowest yield and ultimate strengths ( $162 \pm 2$  MPa and  $252 \pm 3$  MPa, respectively) and the largest ductility ( $8.7\% \pm 0.2\%$ ).

The high strength of the Al-20Si as-built SLM alloy can be attributed to the effect of grain refinement. The effect of grain size on the mechanical properties can be rationalized using the Hall-Petch equation, as already done for the Al-12Si processed by SLM [15]. Structural refinement leads to the reduction of distance between the Si particles that can give a considerable contribution to the strength because the Al/Si interface can effectively reduce the movement of dislocations [32–34]. The decrease of strength after heat treatment is due to the coarsening of the microstructure: the size of the Si particles increases and, consequently, the distance between the particles increases significantly. The increased distance between adjacent Si particles also contributes to the improved ductility of the heat treated samples, as a result of the easier dislocation movement [35].

### 3. Experimental Section

An SLM 250 HL device from SLM solutions equipped with a Yb-YAG laser was used for preparing Al-20Si (wt.%) samples in the form of cylindrical tensile bars with total length of 52 mm, and length and diameter of the gauge length of 17.5 and 3.5 mm. The SLM samples were processed from Al-20Si gas atomized powders using the following processing parameters: scanning speed 1455 mm/s for the volume and 1939 mm/s for the contour, power 320 W for both volume and contour, layer thickness 50  $\mu$ m, hatch spacing 110  $\mu$ m and hatch style rotation of 73°. High purity argon gas was used to ventilate the chamber before and during the building process to minimize oxygen contamination during processing. The SLM samples were then annealed for 6 h at 473 K, 573 K, and 673 K. For comparison, the Al-20Si alloy was processed by graphite mold casting.

The microstructure of the cast, as-built SLM and heat treated SLM samples were characterized by optical microscopy (OM) using an Olympus optical microscope and by scanning electron microscopy (SEM) using a Gemini 1530 microscope coupled with an energy dispersive spectroscopy (EDS) detector. For the microstructural investigations, the specimens were grinded and polished and then etched with a 0.5% HF solution. Image J software was used to calculate the average sizes of the Si particles from the SEM images. Phase analysis was done by X-ray diffraction (XRD) using a D3290 PANalyticalX'pert PRO with Co-K $\alpha$  radiation ( $\lambda = 0.17889$  nm) in reflection geometry. Room temperature tensile tests were performed at a constant strain rate of  $1 \times 10^{-4} \text{ s}^{-1}$  using an Instron 5869 testing device equipped with a laser extensometer (Fiedler Optoelektronik GmbH, Luetzen, Germany). At least three specimens for each condition were tested in order to ensure the reproducibility of the results.

#### 4. Conclusions

The effects of heat treatment on microstructure and the tensile properties of the Al-20Si alloy processed by SLM have been investigated. The size of the eutectic and particulate Si is refined by the SLM processing. The Si particles become coarser and the fibrous eutectic silicon gradually transforms into particulate form with increasing the annealing temperature. The tensile properties of the Al-20Si alloy are dependent on the heat treatment temperature. The UTS and the ductility of the analyzed samples varies from 506 MPa and 1.6% for the as-built SLM material to 252 MPa and 8.7% for the SLM sample heat treated at 673 K. The strength of the Al-20Si SLM materials is very high when compared to the same alloy produced by different techniques, such as casting and extrusion, even for the heat-treated specimens. Therefore, the microstructural variations induced by the heat treatment can be used to tune and optimize the mechanical performance of the Al-20Si SLM parts making them competitive with respect to alloys produced by conventional processing routes.

#### Acknowledgments

This work was supported by the National Natural Science Foundation of China (No. 51001041 and No. 51171054).

#### Conflict of Interest

The authors declare no conflict of interest.

#### References

1. Yadroitsev, I.; Bertrand, P.; Smurov, I. Parametric analysis of the selective laser melting process. *Appl. Surf. Sci.* **2007**, *253*, 8064–8069.
2. Louvis, E.; Fox, P.; Sutcliffe, C.J. Selective laser melting of aluminium components. *J. Mater. Process. Technol.* **2011**, *211*, 275–284.
3. Olakanmi, E.O. Selective laser sintering/melting (SLS/SLM) of pure Al, Al-Mg, and Al-Si powders: Effect of processing conditions and powder properties. *J. Mater. Process. Technol.* **2013**, *213*, 1387–1405.

4. Yadroitsev, I.; Thivillon, L.; Bertrand, P.; Smurov, I. Strategy of manufacturing components with designed internal structure by selective laser melting of metallic powder. *Appl. Surf. Sci.* **2007**, *254*, 980–983.
5. Thijs, L.; Verhaeghe, F.; Craeghs, T.; Humbeeck, J.V.; Kruth, J.P. A study of the microstructural evolution during selective laser melting of Ti-6Al-4V. *Acta Mater.* **2010**, *58*, 3303–3312.
6. Zhang, B.C.; Liao, H.L.; Coddet, C. Effects of processing parameters on properties of selective laser melting Mg-9%Al powder mixture. *Mater. Des.* **2012**, *34*, 753–758.
7. Chlebus, E.; Kuźnicka, B.; Kurzynowski, T.; Dybała, B. Microstructure and mechanical behaviour of Ti-6Al-7Nb alloy produced by selective laser melting. *Mater. Charact.* **2011**, *62*, 488–495.
8. Pantelakis, S.G.; Alexopoulos, N.D. Assessment of the ability of conventional and advanced wrought aluminum alloys for mechanical performance in light-weight applications. *Mater. Des.* **2008**, *29*, 80–91.
9. Jia, Y.D.; Cao, F.Y.; Ning, Z.L.; Guo, S.; Ma, P.; Sun, J.F. Influence of second phases on mechanical properties of spray-deposited Al-Zn-Mg-Cu alloy. *Mater. Des.* **2012**, *40*, 536–540.
10. Polmear, I.J. Aluminum alloys—A century of age hardening. *Mater. Forum* **2004**, *28*, 1–14.
11. Bourell, D.; Wohler, M.; Harlan, N.; Das, S.; Beaman, J. Powder densification maps in selective laser sintering. *Adv. Eng. Mater.* **2002**, *4*, 663–669.
12. Li, J.P.; Wilson, C.; Wijn, J.R.; VanBlitterswijk, C.A.; de Groot, K. Fabrication of porous Ti6Al4V with designed structure by rapid prototyping technology. *Key Eng. Mater.* **2007**, *330*, 1293–1296.
13. Pauly, S.; Löber, L.; Petters, R.; Stoica, M.; Scudino, S.; Kühn, U.; Eckert, J. Processing metallic glasses by selective laser melting. *Mater. Today* **2013**, *16*, 37–41.
14. Thijs, L.; Kempen, K.; Kruth, J.P.; Humbeeck, J.V. Fine-structured aluminium products with controllable texture by selective laser melting of pre-alloyed AlSi10Mg powder. *Acta Mater.* **2013**, *61*, 1809–1819.
15. Prashanth, K.G.; Scudino, S.; Klauss, H.J.; Surreddi, K.B.; Loeber, L.; Wang, Z.; Chaubey, A.K.; Kühn, U.; Eckert, J. Microstructure and mechanical properties of Al-12Si produced by selective laser melting: Effect of heat treatment. *Mater. Sci. Eng. A* **2013**, *590*, 153–160.
16. Chirita, G.; Stefanescu, I.; Soares, D.; Silva, F.S. Influence of vibration on the solidification behaviour and tensile properties of an Al-18 wt%Si alloy. *Mater. Des.* **2009**, *30*, 1575–1580.
17. Hong, S.J.; Suryanarayana, C.; Chun, B.S. Section-dependent microstructure and mechanical properties of rapidly solidified and extruded Al-20Si alloy. *Mater. Res. Bull.* **2004**, *39*, 465–474.
18. Abramov, V.O.; Abramov, O.V.; Straumal, B.B.; Gust, W. Hypereutectic Al-Si based alloys with a thixotropic microstructure produced by ultrasonic treatment. *Mater. Des.* **1997**, *18*, 323–326.
19. Nikanorov, S.P.; Volkov, M.P.; Gurin, V.N.; Burenkov, Y.A.; Derkachenko, L.I.; Kardashev, B.K.; Regel, L.L.; Wilcox, W.R. Structural and mechanical properties of Al-Si alloys obtained by fast cooling of a levitated melt. *Mater. Sci. Eng. A* **2005**, *390*, 63–69.
20. Bendijk, A.; Delhez, R.; Katgerman, L.; de Keijser, Th.H.; Mittemeijer, E.J.; Vanderpers, N.M. Characterization of Al-Si-alloys rapidly quenched from the melt. *J. Mater. Sci.* **1980**, *15*, 2803–2810.

21. Milligan, J.; Vintila, R.; Brochu, M. Nanocrystalline eutectic Al-Si alloy produced by cryomilling. *Mater. Sci. Eng. A* **2009**, *508*, 43–49.
22. Massalski, T.B. *Binary Alloy Phase Diagram*; ASM International: Metals Park, OH, USA, 1986.
23. Flemings, M.C. *Solidification Processing*; McGraw-Hill: New York, NY, USA, 1974.
24. Gremaud, M.; Allen, D.R.; Rappaz, M.; Perepezko, J.H. The development of nucleation controlled microstructures during laser treatment of Al-Si alloys. *Acta Mater.* **1996**, *44*, 2669–2681.
25. Pei, Y.T.; de Hossien, J.Th.M. Functionally graded materials produced by laser cladding. *Acta Mater.* **2000**, *48*, 2617–2624.
26. Wong, T.T.; Liang, G.Y.; Tang, C.Y. The surface character and substructure of aluminium alloys by laser-melting treatment. *J. Mater. Process. Technol.* **1997**, *66*, 172–178.
27. Yeh, J.W.; Yuan, S.Y.; Peng, C.H. A reciprocating extrusion process for producing hypereutectic Al-20wt.% Si wrought alloys. *Mater. Sci. Eng. A* **1998**, *252*, 212–221.
28. Choi, H.; Konishi, H.; Li, X.C. Al<sub>2</sub>O<sub>3</sub> nanoparticles induced simultaneous refinement and modification of primary and eutectic Si particles in hypereutectic Al-20Si alloy. *Mater. Sci. Eng. A* **2012**, *541*, 159–165.
29. Xu, C.L.; Jiang, Q.C. Morphologies of primary silicon in hypereutectic Al-Si alloys with melt overheating temperature and cooling rate. *Mater. Sci. Eng. A* **2006**, *437*, 451–455.
30. Kilicaslan, M.F.; Lee, W.R.; Lee, T.H.; Sohn, Y.; Hong, S.J. Effect of Sc addition on the microstructure and mechanical properties of as-atomized and extruded Al-20Si alloys. *Mater. Lett.* **2012**, *71*, 164–167.
31. Yoon, S.C.; Hong, S.J.; Hong, S.I.; Kim, H.S. Mechanical properties of equal channel angular pressed powder extrudates of a rapidly solidified hypereutectic Al-20 wt% Si alloy. *Mater. Sci. Eng. A* **2007**, *449–451*, 966–970.
32. Scudino, S.; Liu, G.; Sakaliyska, M.; Surreddi, K.B.; Eckert, J. Powder metallurgy of Al-based metal matrix composites reinforced with  $\beta$ -Al<sub>3</sub>Mg<sub>2</sub> intermetallic particles: Analysis and modeling of mechanical properties. *Acta Mater.* **2009**, *57*, 4529–4538.
33. Gurland, J. The fracture strength of sintered tungsten carbide-cobalt alloys in relation to composition and particle spacing. *Trans. Met. Soc. AIME* **1963**, *227*, 1146–1149.
34. Underwood, E.E. *Metals Handbook*, 9th ed.; ASM International: Metals Park, OH, USA, 1985.
35. Cui, X.G.; Cui, C.Y.; Cheng, X.N.; Xu, X.J.; Lu, J.Z.; Hu, J.D.; Wang, Y.M. Microstructure and tensile properties of the sub-micro and nano-structured Al produced by laser surface melting. *Mater. Sci. Eng. A* **2010**, *527*, 7400–7406.